Front. Optoelectron. 2020, 13(4): 318–326
https://doi.org/10.1007/s12200-020-1068-1

RESEARCH ARTICLE

Super-resolution imaging of the dynamic cleavage of intercellular tunneling nanotubes

Wanjun GONG[#], Wenhui PAN[#], Ying HE, Meina HUANG, Jianguo ZHANG, Zhenyu GU, Dan ZHANG, Zhigang YANG (✉), Junle QU

Key Laboratory of Optoelectronic Devices and Systems of Ministry of Education and Guangdong Province, College of Physics and Optoelectronic Engineering, Shenzhen University, Shenzhen 518060, China

© Higher Education Press 2020

Abstract As a new method of cell–cell communication, tunneling nanotubes (TNTs) play important roles in cell–cell signaling and mass exchanges. However, a lack of powerful tools to visualize dynamic TNTs with high temporal/spatial resolution restricts the exploration of their formation and cleavage, hindering the complete understanding of its mechanism. Herein, we present the first example of using stochastic optical reconstruction microscopy (STORM) to observe the tube-like structures of TNTs linking live cells with an easily prepared fluorescent dye. Because of this new imaging microscopy, the cleavage process of TNTs was observed with a high spatial resolution.

Keywords super-resolution, tunneling nanotubes (TNTs), live cell

1 Introduction

Intercellular communication is essential for tissue homeostasis, specific cell functions, and responses to external stimulus. Cell–cell communications typically occur through various processes, such as diffusible factors, including cytokines and chemokines, secreted microvesicles, and direct passage through gap junctions [1]. Recently, a new impressive intercellular communication pathway was found that allows long-distance cell–cell contacts via tunneling nanotubes (TNTs) between these cells, which was initially reported in rat pheochromocytoma (PC12)-derived cells [2] and later in other types of cells [2–7]. The TNTs connecting two cells exhibit long tubular structures with diameters of 50–1500 nm and lengths of tens to hundreds of microns, which maintain a continuous cytoplasm membrane between the connecting cells, thus allowing the transportation of numerous cellular components, such as proteins, RNAs, viruses, and organelles, from one cell to another [8–10]. Generally, actin is included in the central composition and a membrane is wrapped outside, which is typically part of the cell membrane. Additionally, TNTs play distinct roles in the modulation of cell death involved not only in the delivery of injured cells [9–12] but also in enhancing the lysis of distant cells [13]. Thus, addressing the dynamic changes of such TNTs will be helpful for understanding the exact events of intercellular communication behaviors.

In recent years, studies on TNTs were performed in normal cells as well as on the pathogenesis of neurodegenerative diseases and cancer [14] mainly via electron and fluorescence microscopy [11,15–19]. However, it is difficult to observe ultra-fine TNTs *in vivo* because of their fragility to light, mechanical stress, or chemical fixation and the limit by the inherent shortcomings of the imaging techniques used. Although electron microscopy is able to provide spatial resolution as high as up to a nanometer, it cannot be used to image live cells [3]. In contrast, optical microscopies can be used to image live cells, but the spatial resolution is less than 200 nm owing to the optical diffraction limit. Since the first report on TNTs, only two kinds of markers targeting tube-like structures have emerged, including wheat germ agglutinin (WGA)-chromophore binding for cell membrane and phalloidin-chromophore targeting for F-actin. Both derivatives are expensive and difficult to purify [3,20,21]. Stochastic optical reconstruction microscopy (STORM) [22–24] is an advanced super-resolution imaging technique that offers promising potential to carry out biological imaging of dynamic TNTs between live cells. Together with special optical probes, it is possible to perform STORM imaging

Received July 18, 2020; accepted September 11, 2020

E-mail: zhgyang@szu.edu.cn

[#]These authors contributed equally to this work.

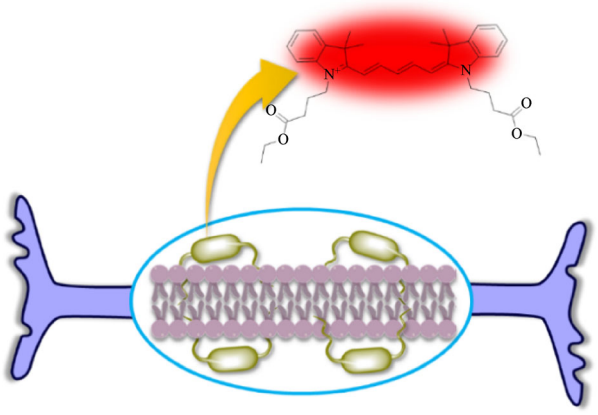

Fig. 1 Diagram of the proposed labeling method for probe **1** on TNTs

of dynamic TNTs between live cells. However, the lack of excellent STORM probes makes it difficult to observe the ultra-fine structures of TNTs in the natural environment. Until now, there have been no reports on super-resolution imaging of dynamic TNTs between live cells.

In this study, we designed a simple cyanine-based probe to label TNTs and to perform STORM imaging. The probe was composed of a Cy5 dye with a two-ester moiety at the N-position (Fig. 1). It was characterized using nuclear magnetic resonance (NMR) and mass spectra (See Supplementary Information). Then, the probe was used to label the TNTs and carry out STORM imaging to study the cleavage of the TNTs and the ultra-fine details of dynamic changes.

2 Experimental

First, we synthesized probe **1** via a simple reaction method with high yields. In detail, **1** was prepared by heating 2,3, 3-trimethylindolenine and an equivalent amount of 4-bromobutyric acid ethyl ester in acetonitrile solution. The obtained quaternary ammonium salt was subsequently heated with condensation reagent in Ac_2O/NaOAc for 30 min. The obtained blue residue was further purified using a silica column, and the synthetic details and structure identification of the probe and intermediate are provided in the Supplementary Information [25–27].

3 Discussion

The photophysical behaviors of **1** were tested to confirm the feasibility of the probe for TNT imaging. The absorption and fluorescent emission spectra of **1** were measured in ethanol to show the peaks at λ_{abs} = 654 nm and λ_{em} = 679 nm, respectively (Figs. 2(a) and S1), indicating that the probe can be excited at 656 nm wavelength.

A home-built STORM optical setup was used to measure the transient photoblinking of **1** under illumination of a single laser beam (656 nm) with a power density of 0.682 kW/cm^2. The marked photoblinking of **1** was observed with a high photon number (6000–8000) and larger on–off duty cycle (*ca.* 0.00126) than that of Alexa 647 [26]. It could be switched between fluorescence on and off states and remained in the dark state for a sufficiently long time, which is suitable for single molecule localization-based STORM imaging. Additionally, the duration of photoblinking of probe **1** could last for more than 800 s with a suitable switching frequency (Fig. 2(c)), and over 60% of probe molecules survived after a 700 s illumination period (Fig. 2(b)), which made it possible for long-term observation of the dynamic behaviors of live cells.

The cytotoxicity of probe **1** was further studied to assess the impact on the dynamics of TNTs, including the formation or cleavage processes. HeLa cells were cultured with **1** at different concentrations (1.0, 2.0, and 4.0 μmol/L) for different time periods (1, 5, and 10 h) (Fig. 3(e)). Most of the cells survived and were active at the concentration of 4.0 μmol/L for even 10 h of incubation. This showed that the probe exhibited rare toxicity to HeLa cells, which was favorable for live cell imaging. As biological dynamic changes in live cells usually last for several minutes, a fluorescent probe without cytotoxicity would be extremely important to the study of natural biological processes.

After accomplishing all primary tests, super-resolution imaging of TNTs was further performed on the STORM setup using HeLa and COS-7 cells to identify the exact location of **1** in the live cells. After the probe was incubated with COS-7 cells for 15 min, the sample was washed with phosphate buffer saline (PBS) and then placed on the sample stage of the STORM system to check the photoblinking in live cells. The specimen was illuminated with a single laser beam at 656 nm with a power density of 200 mW/cm^2. As shown in Figs. 4(a) and S2(a), according to the wide-field image, the fluorescent probe mainly stained the long tube between two COS-7 cells but could not provide fine details of the TNTs. The photoblinking images of the probe were recorded using an electron multiplying charge coupled device (EMCCD, 60 Hz). A super-resolved image was reconstructed using 200 frames with a reconstruction algorithm of the fast localization algorithm based on the continuous-space formulation (FALCON) for high-density super resolution [28]. As shown in Figs. 4 and S2, we acquired the STORM images of the TNTs between COS-7 cells, exhibiting thin and long tube structures. Compared with the wide-field images, the STORM images showed a clear linear structure of the TNTs, which could be used to quantify the thickness of the tubes.

To further disclose the TNT dynamic change, the FALCON algorithm was used to reconstruct the dynamic STORM images of the TNTs using 180 frames with a step gap of 20 frames (3 s temporal resolution). As

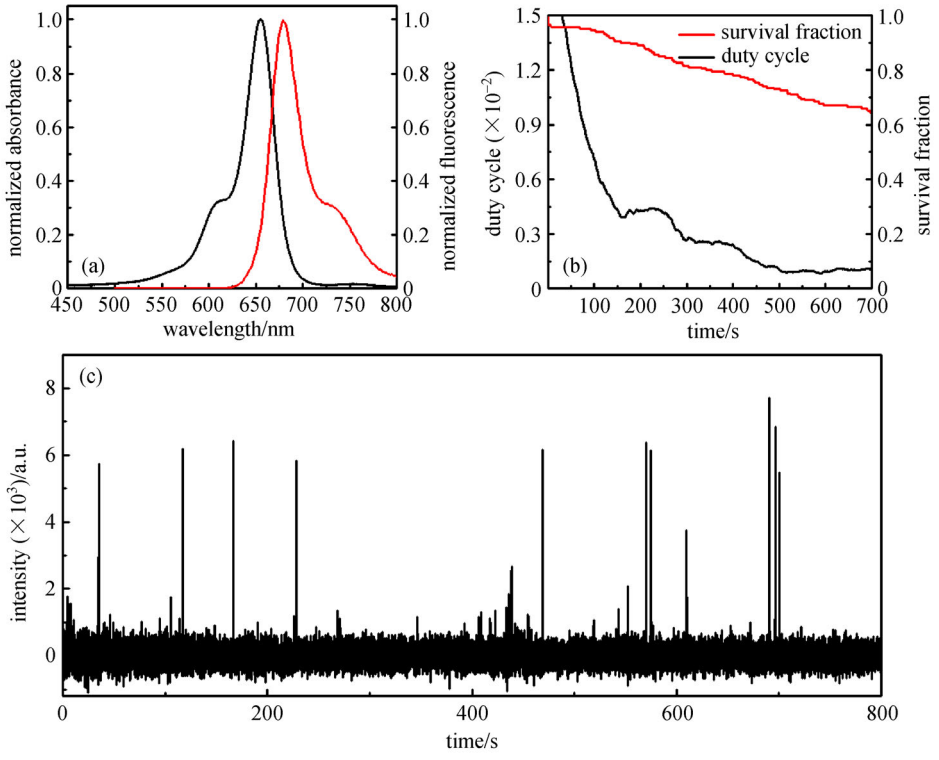

Fig. 2 Photophysical properties of probe **1** were evaluated. (a) Excitation and emission spectra of probe **1** (black and red curves, respectively), with a laser excitation wavelength of 633 nm. (b) Duty cycle calculated for probe **1**. (c) Single-molecule fluorescence time traces measured in the absence of βME and oxygen-scavenging system

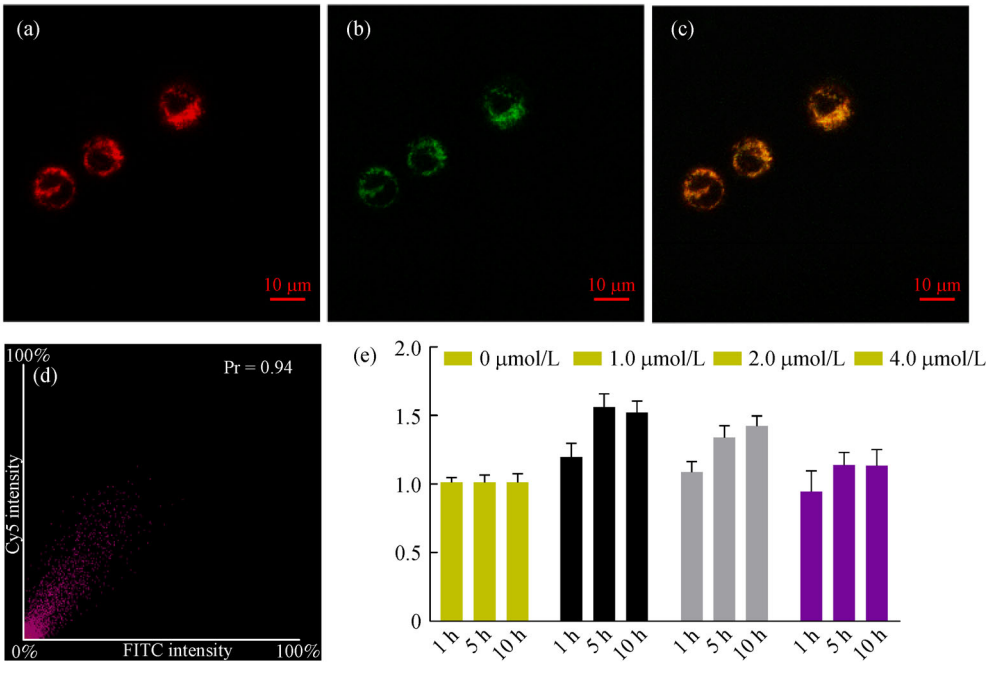

Fig. 3 Fluorescent imaging of the probe in HeLa cells. The co-localization experiment was conducted by co-incubating **1** (1 μmol/L) (a) with a commercially available dye, membrane tracker-Dioctadecylcarbocyanines (DIO) (1 μmol/L) (b). The merged image (c) and Pr coefficient (d) was obtained by overlapping (a) and (b); FITC is the abbreviation of fluoresceinthioisocyanate. (e) Cell viability experiment on HeLa cells when incubating with probe **1**

demonstrated in Figs. 4(a) and S2(b)–S2(f), a consecutive change in the TNT with ultra-fine structures was obtained to show the detailed changes of TNT cleavage. From the magnified image of the region of interest, as indicated by the dashed box in Figs. 4(b) and 4(c), a clear cleavage of the TNTs and some interesting features could be observed (see Electronic Supplementary Videos S1 and S2). First, the breakage of the TNTs started at 46 s from the right end; and on the left side of the TNT, it slowly shrunk and finally formed a circle (Fig. 4(b)). A zoomed in picture of the cleavage site of TNT is shown in Fig. 4(c), from which we observed the initial TNT to be a linear structure, and later, the breaking site showed up with a circle formed at the right end with an increase in diameter of the circle. Meanwhile, cleavage occurred at the left end of the circle. In the wide-field image, the circle ring is totally a solid flat disc with a diameter of 530.1±14.1 nm, which is considerably larger than the optical diffraction limit; however, in the STORM image, the solid circle became a hollow ring with an full width at half maximum (FWHM) value of 133.5±1.5 nm, as calculated by Gaussian fitting (Figs. 4(d) and 4(e)). This provides a promising chance to study the biological functions of TNTs.

4 Conclusions

We developed a simple Cy5-based probe for STORM imaging of intercellular tunneling nanotubes. The probe, which has two ethyl-butyrate groups that can be used as TNT membrane binding sites, kept photoblinking and remained photostable for long-term STORM imaging. Using this probe, the typical TNT ring-like structure with a diameter of 133.5±1.5 nm formed during the cleavage of the TNTs was observed by STORM imaging, which provided the first view of TNTs cleaving in live cells. To the best of our knowledge, this is the first report on a simple probe for STORM imaging of TNT dynamics, particularly for the analysis of its formation and functional roles in cell communication.

Acknowledgements This work has been partially supported by the National Natural Science Foundation of China (Grant Nos. 61875131, 61525503, 61620106016, and 61835009), Shenzhen Basic Research Project (Nos. JCYJ20170818100931714, JCYJ20180305125549234, and JCYJ20170412105003520), and Shenzhen International Cooperation Research Project (No. GJHZ20180928161811821).

Electronic Supplementary Material Supplementary material is available

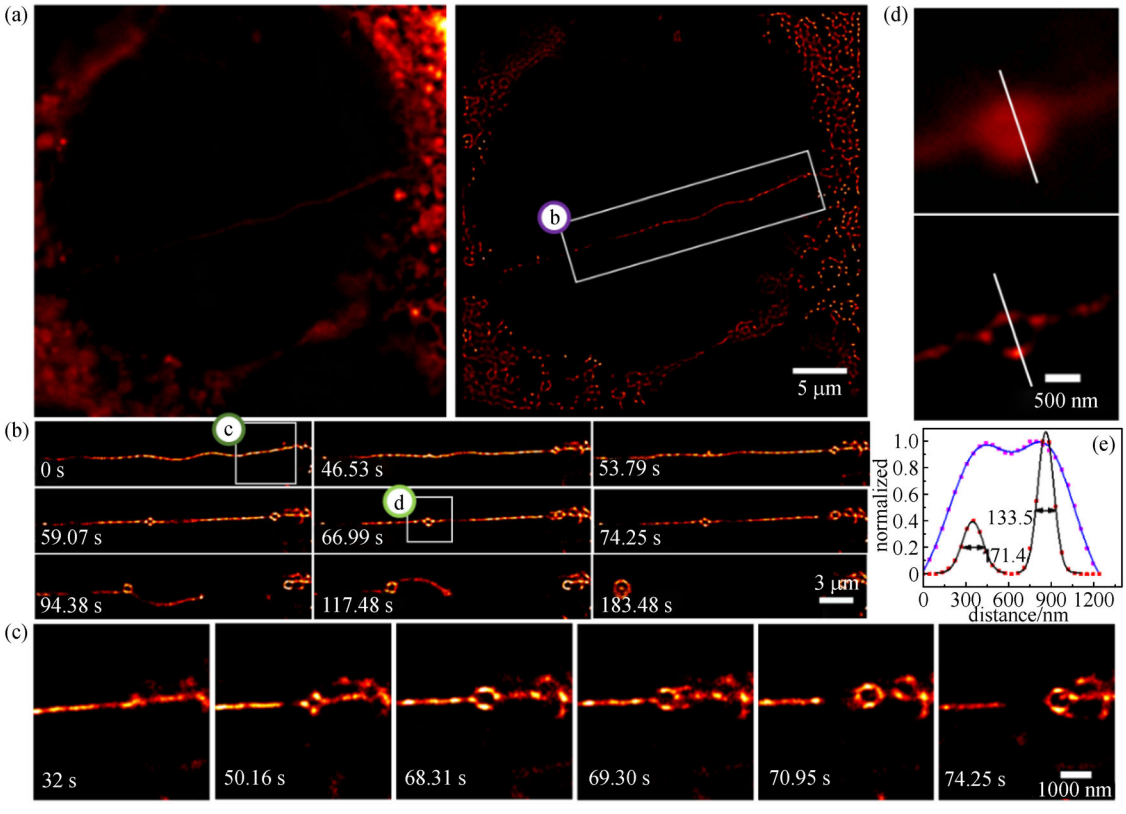

Fig. 4 STORM imaging of TNTs and their dynamic changes. (a) One snapshot (t = 0 s) from a 184-s movie (left) and a reconstructed STORM image from 180 frames recorded over 3 s. (b) and (c) Time-series STORM snapshots of intercellular filament dynamics. Each image was reconstructed from 180 frames recorded over 3 s. (d) Magnified images of the circle in the square in (b) obtained by wide-field and STORM imaging. (e) Fluorescence intensity profiles along the white lines in (d). The black line shows the signal in the STORM image, whereas the blue line shows the signal in the wide-field image. FWHM values of these profiles are 133.5±1.5 nm (super-resolution image) and 530.1±14.1 nm (wide-field image), respectively

in the online version of this article at https://doi.org/10.1007/s12200-020-1068-1 and is accessible for authorized users.

References

1. Sattentau Q. Avoiding the void: cell-to-cell spread of human viruses. Nature Reviews Microbiology, 2008, 6(11): 815–826
2. Sherer N M, Lehmann M J, Jimenez-Soto L F, Horensavitz C, Pypaert M, Mothes W. Retroviruses can establish filopodial bridges for efficient cell-to-cell transmission. Nature Cell Biology, 2007, 9 (3): 310–315
3. Rustom A, Saffrich R, Markovic I, Walther P, Gerdes H H. Nanotubular highways for intercellular organelle transport. Science, 2004, 303(5660): 1007–1010
4. Wang X, Veruki M L, Bukoreshtliev N V, Hartveit E, Gerdes H H. Animal cells connected by nanotubes can be electrically coupled through interposed gap-junction channels. Proceedings of the National Academy of Sciences of the United States of America, 2010, 107(40): 17194–17199
5. Hase K, Kimura S, Takatsu H, Ohmae M, Kawano S, Kitamura H, Ito M, Watarai H, Hazelett C C, Yeaman C, Ohno H. M-Sec promotes membrane nanotube formation by interacting with Ral and the exocyst complex. Nature Cell Biology, 2009, 11(12): 1427–1432
6. Zhu D, Tan K S, Zhang X, Sun A Y, Sun G Y, Lee J C. Hydrogen peroxide alters membrane and cytoskeleton properties and increases intercellular connections in astrocytes. Journal of Cell Science, 2005, 118(16): 3695–3703
7. Wang X, Bukoreshtliev N V, Gerdes H H. Developing neurons form transient nanotubes facilitating electrical coupling and calcium signaling with distant astrocytes. PLoS One, 2012, 7(10): e47429
8. Önfelt B, Nedvetzki S, Benninger R K P, Purbhoo M A, Sowinski S, Hume A N, Seabra M C, Neil M A A, French P M W, Davis D M. Structurally distinct membrane nanotubes between human macrophages support long-distance vesicular traffic or surfing of bacteria. Journal of Immunology (Baltimore, Md.: 1950), 2006, 177(12): 8476–8483
9. Cselenyák A, Pankotai E, Horváth E M, Kiss L, Lacza Z. Mesenchymal stem cells rescue cardiomyoblasts from cell death in an *in vitro* ischemia model via direct cell-to-cell connections. BMC Cell Biology, 2010, 11(1): 29
10. Naphade S, Sharma J, Gaide Chevronnay H P, Shook M A, Yeagy B A, Rocca C J, Ur S N, Lau A J, Courtoy P J, Cherqui S. Brief reports: lysosomal cross-correction by hematopoietic stem cell-derived macrophages via tunneling nanotubes. Stem Cells (Dayton, Ohio), 2015, 33(1): 301–309
11. Wang X, Gerdes H H. Transfer of mitochondria via tunneling nanotubes rescues apoptotic PC12 cells. Cell Death and Differentiation, 2015, 22(7): 1181–1191
12. Osswald M, Jung E, Sahm F, Solecki G, Venkataramani V, Blaes J, Weil S, Horstmann H, Wiestler B, Syed M, Huang L, Ratliff M, Karimian Jazi K, Kurz F T, Schmenger T, Lemke D, Gömmel M, Pauli M, Liao Y, Häring P, Pusch S, Herl V, Steinhäuser C, Krunic D, Jarahian M, Miletic H, Berghoff A S, Griesbeck O, Kalamakis G, Garaschuk O, Preusser M, Weiss S, Liu H, Heiland S, Platten M, Huber P E, Kuner T, von Deimling A, Wick W, Winkler F. Brain tumour cells interconnect to a functional and resistant network. Nature, 2015, 528(7580): 93–98
13. Chauveau A, Aucher A, Eissmann P, Vivier E, Davis D M. Membrane nanotubes facilitate long-distance interactions between natural killer cells and target cells. Proceedings of the National Academy of Sciences of the United States of America, 2010, 107 (12): 5545–5550
14. Lou E, Fujisawa S, Morozov A, Barlas A, Romin Y, Dogan Y, Gholami S, Moreira A L, Manova-Todorova K, Moore M A. Tunneling nanotubes provide a unique conduit for intercellular transfer of cellular contents in human malignant pleural mesothelioma. PLoS One, 2012, 7(3): e33093
15. Austefjord M W, Gerdes H H, Wang X. Tunneling nanotubes: diversity in morphology and structure. Communicative & Integrative Biology, 2014, 7(1): e27934
16. Dubois F, Jean-Jacques B, Roberge H, Bénard M, Galas L, Schapman D, Elie N, Goux D, Keller M, Maille E, Bergot E, Zalcman G, Levallet G. A role for RASSF1A in tunneling nanotube formation between cells through GEFH1/Rab11 pathway control. Cell Communication and Signaling, 2018, 16(1): 66
17. Sun X, Wang Y, Zhang J, Tu J, Wang X J, Su X D, Wang L, Zhang Y. Tunneling-nanotube direction determination in neurons and astrocytes. Cell Death & Disease, 2012, 3(12): e438
18. Tang B L. Unconventional secretion and intercellular transfer of mutant huntingtin. Cells, 2018, 7(6): 59
19. Weng Z, Zhang B, Tsilioni I, Theoharides T C. Nanotube formation: a rapid form of "alarm signaling"? Clinical Therapeutics, 2016, 38 (5): 1066–1072
20. Omsland M, Pise-Masison C, Fujikawa D, Galli V, Fenizia C, Parks R W, Gjertsen B T, Franchini G, Andresen V. Inhibition of tunneling nanotube (TNT) formation and human T-cell leukemia virus type 1 (HTLV-1) transmission by cytarabine. Scientific Reports, 2018, 8(1): 11118
21. Delage E, Cervantes D C, Pénard E, Schmitt C, Syan S, Disanza A, Scita G, Zurzolo C. Differential identity of filopodia and tunneling nanotubes revealed by the opposite functions of actin regulatory complexes. Scientific Reports, 2016, 6(1): 39632
22. Rust M J, Bates M, Zhuang X. Sub-diffraction-limit imaging by stochastic optical reconstruction microscopy (STORM). Nature Methods, 2006, 3(10): 793–796
23. Bates M, Huang B, Dempsey G T, Zhuang X. Multicolor super-resolution imaging with photo-switchable fluorescent probes. Science, 2007, 317(5845): 1749–1753
24. Huang B, Wang W, Bates M, Zhuang X. Three-dimensional super-resolution imaging by stochastic optical reconstruction microscopy. Science, 2008, 319(5864): 810–813
25. Wang B, Fan J, Sun S, Wang L, Song B, Peng X. 1-(Carbamoylmethyl)-3H-indolium squaraine dyes: synthesis, spectra, photo-stability and association with BSA. Dyes and Pigments, 2010, 85(1–2): 43–50
26. Roberts R M, Edwards M B. Acetoacetic ester-type cleavage by aniline1. Journal of the American Chemical Society, 1950, 72(12): 5537–5539

27. Loeber D E, Russell S W, Toube T P, Weedon B C L, Diment J. Carotenoids and related compounds. Part XXVIII. Synthesis of zeaxanthin, -cryptoxanthin, and zeinoxanthin (-cryptoxanthin). Journal of the Chemical Society C: Organic, 1971, 404–408
28. Min J, Vonesch C, Kirshner H, Carlini L, Olivier N, Holden S, Manley S, Ye J C, Unser M. FALCON: fast and unbiased reconstruction of high-density super-resolution microscopy data. Scientific Reports, 2014, 4(1): 4577

Wanjun Gong graduated from Wuhan University of Science and Technology, China in 2017 and received his Ph.D. degree majored in Supramolecular Chemistry. Then he joined Prof. Junle Qu's group in College of Physics and Optoelectronic Engineering, Shenzhen University, China as a postdoctor, in which group he was concentrated on the construction of organic fluorescent probes for super resolution imaging. His current research interests include but are not limited to advanced organic fluorophore design and synthesis.

Wenhui Pan obtained her master degree under the supervision of Prof. Zhigang Yang at Shenzhen University, China in 2020. Her research interests mainly focus on super-resolution imaging microscopy and its biological applications.

Ying He graduated from Zhejiang University, China in 2013. Now he works in College of Physics and Optoelectronic Engineering, Shenzhen University, China as an Associate Research Fellow. His current research interests include but are not limited to super-resolution imaging and fluorescence lifetime imaging.

Meina Huang received her Ph.D. degree from College of Chemistry and Chemical Engineering, Guangxi University, China in 2018. She joined Prof. Patrick J. Walsh's group in Department of Chemistry, University of Pennsylvania, USA as a training jointly PhD student. In 2018, she worked as a postdoctoral fellow in the research group of Prof. Junle Qu at Shenzhen University, China. Her current research interest mainly focuses on fluorescent materials for fluorescence imaging and super-resolution imaging.

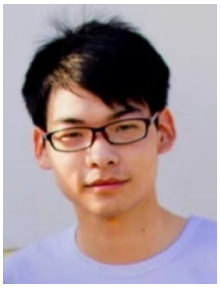

Jianguo Zhang is currently a master student under the supervision of Prof. Zhigang Yang at Shenzhen University, China. His current research interest mainly focuses on fluorescent materials for super-resolution imaging and fluorescence lifetime imaging.

Zhenyu Gu is currently a master student under the supervision of Prof. Zhigang Yang at Shenzhen University, China. His current research focuses on the optical coherence tomography.

Dan Zhang majored in Optoelectronic Information Science and Engineering at College of Physics and Optoelectronic Engineering, Shenzhen University, China during her undergraduate period. She is currently a master student under the supervision of Prof. Zhigang Yang at Shenzhen University, China. Her current research interest mainly focuses on fluorescent materials for super-resolution imaging and fluorescent lifetime imaging.

Zhigang Yang received his Ph.D. degree from Dalian University of Technology, China in 2011. Then he perused his research as a postdoctor and research professor at Korea University (2011–2014), Korea. Since 2015, he became a faculty and is currently an Associate Professor at Shenzhen University, China. Presently, his research interests focus on biological optical imaging, super-resolution optical imaging, fluorescence lifetime imaging and OCT imaging. To date, his research has recorded about 50 scientific publications and 10 patents.

Junle Qu received his Ph.D. degree from Xi'an Institute of Optics and Precision Mechanics, Chinese Academy of Sciences, China in 1998. He is currently a distinguished professor in College of Physics and Optoelectronic Engineering at Shenzhen University, China. He is currently a director of Center for Biomedical Photonics. His research interests cover biomedical

photonics and biological imaging, phototherapy, biophotonics and nanophotonics. To date, he has published over 300 scientific publications and 30 patents.

Supplementary Information

Chemical synthesis

All reactions were performed in oven-dried glassware, and solvent used was analytical or high performance liquid chromatography (HPLC) grade. All the reagents were obtained from commercial suppliers and used without further purification. A rotary evaporator was used to concentrate the reaction mixtures. Thin layer chromatography (TLC) was performed using glass-backed sheets of silica gel and visualized under a UV lamp of 254 and 365 nm. Column chromatography was performed to purify compounds using silica gel 60 (200–400 mesh).

Synthesis of 1

2 (3.5 g, 10 mmol) and malonaldehyde dianilide hydrochloride (2.6 g, 10 mmol) were mixed in a round-bottom flask, then anhydrous NaOAc (0.82 g, 10 mmol) and Ac_2O (10 mL) were added. The mixture was then heated at 100°C till the reaction mixture turned blue. After 30 min, the reaction was stopped by removing heating and was allowed to cool to room temperature. The reaction mixture was poured into diethyl ether (150 mL). The solid was filtered and washed with brine, after dried over anhydrous Na_2SO_4 and evaporated solvent, the obtained residue was purified with column chromatography (silica gel; DCM/MeOH 20:1 *v*/*v*) to give product 2 with a metallic luster (59% yield).

^{1}H NMR (300 MHz, DMSO-d_6) δ 8.35 (t, J = 13.1 Hz, 2H), 7.61 (d, J = 7.4 Hz, 2H), 7.46–7.29 (m, 4H), 7.24 (td, J = 4.8, 2.7 Hz, 2H), 6.60–6.48 (m, 1H), 6.35 (d, J = 14.0 Hz, 2H), 4.06 (dq, J = 14.2, 7.4 Hz, 8H), 3.32 (s, 4H), 1.92 (t, J = 7.1 Hz, 4H), 1.68 (s, 12H), 1.16 (t, J = 7.1 Hz, 6H). ^{13}C NMR (75 MHz, $CDCl_3$) δ 172.91, 153.78, 142.09, 141.12, 128.74, 125.12, 122.21, 119.93, 110.79, 104.03, 68.35, 60.81, 49.40, 43.61, 30.73, 22.87, 22.18, 14.25. ESI-MS: *m*/*z* found: 583.60, Calc: 583.35.

Synthesis of 2

2,3,3-trimethyl-3*H*-indole (7.9 g, 50 mmol) and 4-Bromobutyric acid ethyl ester (9.78 g, 50 mmol) were added to dry MeCN (50 mL) and the solution was heated under reflux for 24 h. After cooling to room temperature, the solid was filtered and washed with MeCN (15 mL × 3) and Et_2O (15 mL × 3). Then the solid was dried under vacuum and used without further purification.

Cell culture

Hela cells and COS-7 cells were maintained in a 5% CO_2 atmosphere at 37°C in RPMI-1640 (Gibco thermofisher scientific), supplemented with 10% fetal bovine serum (Gibco thermofisher scientific). For imaging, cells were plated into confocal dishes. Experiments were started when cells were 70%–80% confluent.

STORM imaging of live cells

For live cell STORM imaging, the probe was added to the cells with a constant concentration of 1.0 μmol/L. After 1 h the cells were washed with HBSS (without phenol red) and incubation for 5 min and repeated for another 2 times. Finally, cells were imaged with dSTORM microscope using live cell STORM imaging buffer (prepared with HBSS (without phenol red) containing 2% glucose, 6.7% of 1 mol/L HEPES (pH 8.0), 0.5% β-mercaptoethanol (Sigma) and an oxygen-scavenging system).

Single molecule localization microscopy (SMLM) was carried out using an inverted microscope (Nikon Ti2-A) with 100×/NA 1.47 oil objective lens and an electron-multiplying charge-coupled device (EMCCD) camera (iXon Ultra 897; Andor). Fluorophores were excited with a 656 nm laser and images were recorded at 16 ms/frame. Super-resolution images were constructed using FALCON algorithm.

Colocalization experiment

For colocalization experiments, cells in confocal dishes were first stained with the probe at the concentration of 0.5 μmol/L in dulbecco's modified eagle's medium

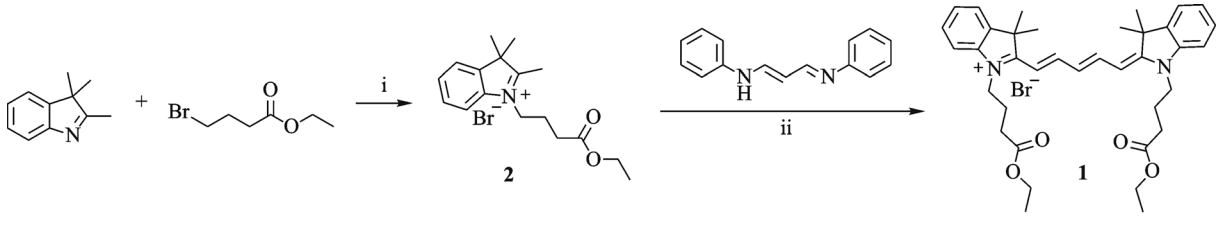

Synthetic route of the target probe and reference compounds; i) MeCN, reflux; ii) Ac_2O/NaOAc, 100°C

(DMEM). After 1 h cells were washed with HBSS (having no phenol red) for 5 min. Following this, cells were treated with either Rhodamin123 (1 μm) or ER tracker green (1 μm) or Lyso tracker green (1 μm) for 35 min and washed with HBSS for 3 times 5 min each. Then the cells were imaged with a laser scanning confocal microscope (Leica SP2) at 633 nm for the probe using HBSS buffer.

Toxicity assay

For cytotoxicity assays, Hela cells were plated at a density of 5000 cells per well. After 18–20 h cells were treated with the probe at different concentrations in serum containing medium and incubated for different time points. Following this CCK8 assay was performed according to the manufacturer's protocol. Absorbance was measured with plate reader at 450 nm microplate reader.

Super-resolution microscopy setup

A home-built STORM system was employed to image TNTs. This system consists of an Olympus IX 81 inverted optical microscope, a 656 nm solid-state laser (460 mW;

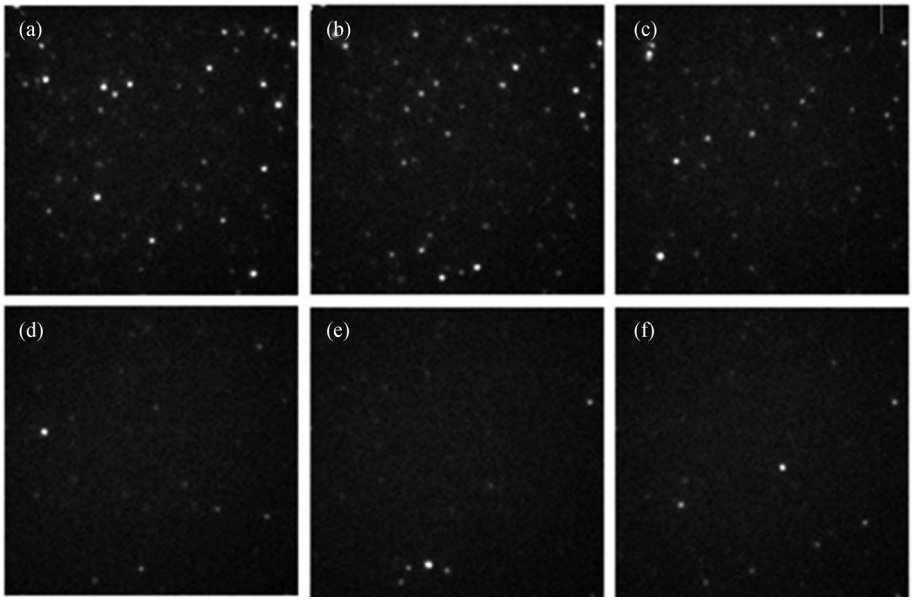

Fig. S1 Reversible and spontaneous fluorescence blinking over tens of seconds in the PBS buffer at different times. (a) 10 s. (b) 150 s. (c) 300 s. (d) 450 s. (e) 600 s. (f) 760 s. The bright spots are still observed under long-time illumination by a laser beam (656 nm)

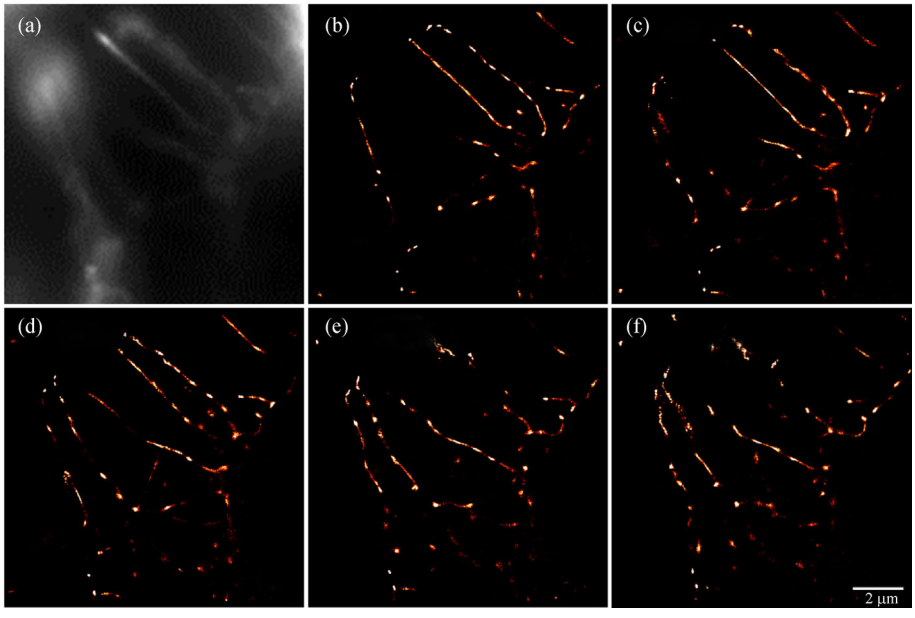

Fig. S2 Wide field imaging (a) of TNTs and STORM imaging of TNTs at different time. (b) 8 s. (c) 40 s. (d) 88 s. (e) 144 s. (f) 196 s

CNI Laser China), a custom dichroic beamsplitter (FF409-Di03/ FF552-Di02; Semrock), a neutral density filter kit (Optical Densities from 0.1 to 4.0, THORLABS), a custom filter set (LED-DA/FI/TR/Cy5-4X4M-B-000; Semrock), a long pass filter (BLP01-488R-25; Semrock) and an EMCCD camera (iXon Ultra 897; Andor).

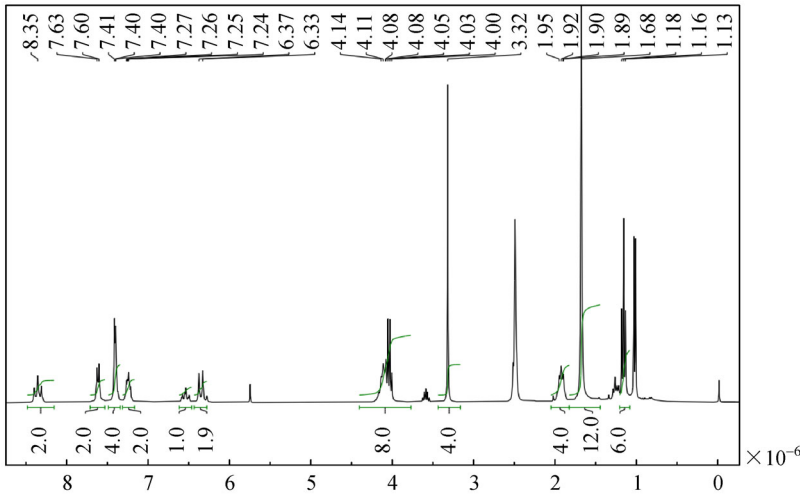

Fig. S3 ^{1}H NMR spectrum for **1**

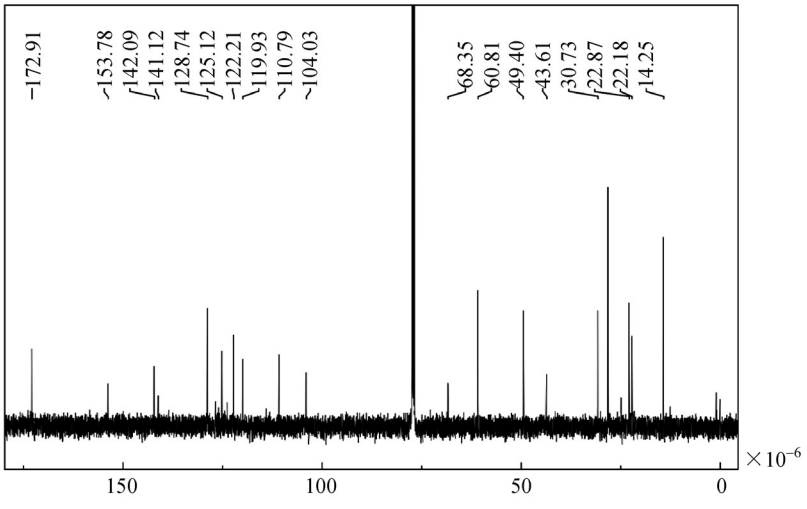

Fig. S4 ^{13}C NMR (300 MHz, $CDCl_3$) spectra of **1**